

MODELLING AND EXPERIMENTS ON STRING/BODY COUPLING AND THE EFFECTIVENESS OF A CELLO WOLF-KILLING DEVICE

Vincent Debut (1), Octavio Inacio (2), Thibaut Dumas (3), Jose Antunes (1)

(1) Instituto Tecnológico e Nuclear, Applied Mechanics Laboratory (ITN/ADL), Sacavem, Portugal

(2) Instituto Politecnico do Porto (IPP), ESMAE, Laboratory of Musical Acoustics, Porto, Portugal

(3) Luthier, Lisbon, Portugal

PACS: 43.75.-z, 43.75.De, 43.75.Gh.

ABSTRACT

A common annoying phenomenon which arises with most cellos and violas is the so-called "wolf note". This is a warbling sound stemming from a severe interaction between the string and the body motions, coupled through the instrument bridge. Instrument builders have found that adding a small auxiliary mass on the so-called "dead" side of the string often inhibits the wolf phenomenon. However, the tuning of such "wolf-eliminators" is often laborious, erratic, if not ineffective, because the physical role of such devices is still poorly understood. Following our previous work on this problem, we address the dynamical behavior of the string/body/wolf-eliminator coupled system, which is studied here in a more systematic manner, both theoretically and through experiments performed on a XIXth century cello. We briefly recall our fully coupled model for this problem, and then perform extensive hand-bow experiments, as well as illustrative computations, which show the effectiveness of this wolf-eliminator as a function of the device mass and location along the dead side of the string. This experimental and numerical work contributes to clarify the functioning of this anti-wolf device and provides guidelines for an effective use.

INTRODUCTION

String players are well aware of a conspicuous annoying and highly unmusical phenomenon, which arises most often with cellos – frequently with the best instruments – which is the so-called “wolf note”. This emerges when the played string length is such that the sounding note approaches the frequency of a particular low-damped body mode. Physically, the resulting warbling sound – often compared to a wolf howling – stems from the severe interaction between the string and the body vibrations, coupled at the instrument bridge.

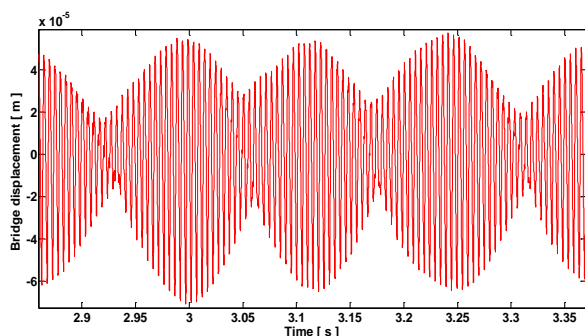


Figure 1. Experimentally recorded cello bridge vibration resulting from a wolf note, for a bowed G string fingered at a position approximately $L/3$ from the bridge.

Then, as shown in Figure 1, a low-frequency beating pervades the system response, while energy transfers from the string to the body and back. However, real physics are more complex than this basic description suggests, as the system is subjected to the highly nonlinear bow/string friction excitation mechanism.



Figure 2. Typical anti-wolf device, mounted on a cello G string between the bridge and tailpiece.

Since many years ago, instrument builders found that adding a small auxiliary mass on the so-called “dead” side of the string (between bridge and tailpiece), as pictured in Figure 2,

often inhibits the wolf phenomenon. However, the tuning of such “wolf-eliminators” – e.g. choosing their optimal mass and best location – is a laborious trial-and-error procedure. Furthermore, their actual effectiveness is often erratic, as the physical role of such devices is still poorly understood.

Theoretical and computational studies on the wolf note started in the late 70s, with the pioneer work by McIntyre, Schumacher and Woodhouse – see McIntyre & Woodhouse (1979) and McIntyre et al. (1983). In their work, coupling with the body dynamics was simulated by implementing the dynamics of a single body mode in their wave-reflection function at the bridge-side boundary of the string. They thus achieved numerical simulations which successfully displayed the basic features of wolf notes. Experiments on this problem are also documented in a few papers, for instance Gough (1980) and Puaud et al. (1991). Although studies on the wolf note became less fashionable, we believe that several important aspects of this problem are still insufficiently understood. The manner in which anti-wolf devices affect the dynamics of the string/body coupled system constitutes one such aspect.

Following our recently published theoretical and experimental work on string/body coupled dynamics – see Inacio & Antunes (2008) and Inacio et al. (2008) – we present in this paper systematic hand-bow experiments, performed on a XIXth century cello. These tests show the effectiveness of this type of wolf-eliminator – or lack of it – as a function of the device mass and location along the dead side of the string. The experimental results are then discussed in the light of our computational model of the bowed string, fully coupled to the body dynamics and to the anti-wolf device.

We briefly recall our approach for achieving time-domain numerical simulations for this problem, which encapsulates a dynamical model of the cello actually tested. In contrast to the computational technique developed by McIntyre, Schumacher and Woodhouse, our computational method enables a rich dynamical model of the instrument body, through the inclusion of many body modes. Furthermore, our approach also enables the modeling of anti-wolf devices, because the dynamics of the “dead-string” region are also accounted in our model.

The illustrative computations provided enable a detailed study of the friction-excited wolf-note regimes of the string/body/eliminator system, including the actual motions of the “dead” side of the string and of the anti-wolf masses. We present computations using several wolf-eliminator masses and mounting locations, which help to elucidate the dynamical behavior of these devices, the manner in which they affect the string/body coupled motions and their ultimate effectiveness as “wolf-killers”.

COMPUTATIONAL MODEL

General approach

As in our previous work, a modal formulation for both the string and the instrument body is used. This enables a very “physical” assembling of the various ingredients, which constitute the fully coupled model of the string/body/eliminator. More specifically, as illustrated in Figure 3:

- The string is described in terms of the transverse modes pertaining to the full length between the tailpiece and the nut.

Their frequencies are therefore lower than those of the “life” string length, between the bridge and the nut. Whatever the

note played, the modal basis used is always the one pertaining to the full-length free string. Both ideal (pure harmonic) real (inharmonic) strings can be modeled with similar ease.

- The body is modeled by its modal properties, as identified through impact tests at the instrument bridge. The properties of these modes thus reflect the overall dynamical behavior of the body, including damping from all possible dissipation mechanisms.

- Coupling between the string and the body is achieved using a penalty formulation, in order to enforce a near-identical motion of the string and the body at the bridge contact location.

- The wolf eliminator is modeled as a point mass, which is coupled to the string through a (more or less) flexible damped fixture. This, also, results in a penalty formulation when coupling the eliminator and the string dynamics at some location in the “dead” side of the string.

- Additionally, we provide a manner of playing any note by constraining the string at any given location by an “artificial finger”, in order to shorten the “active” string length. Again, this is implemented using a penalty formulation. As pointed before, the modal basis used is always the one pertaining to the full-length free string. This approach enables, in particular, the playing of *glissandi* without introducing any numerical artifacts, which proved very convenient for the present study.

- For the purposes of this work, a basic Coulomb-type friction model is used. Actually, all other aspects of our computational model may be easily combined with a more refined friction model, for instance the thermal approach developed by Smith & Woodhouse (2000), therefore this does not constitute a limitation.

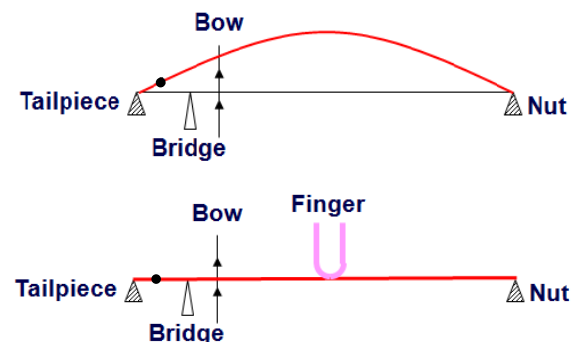


Figure 3. Basic scheme of the string/body/eliminator coupled system, implemented in our computational modal approach. Upper plot: first mode of the string modal basis; Lower plot: “finger” control of the string length and played frequency.

These various aspects will now be detailed in mathematical terms.

String and body dynamics

Consider an ideal string of length L , linear density and dissipation coefficient η , subject to a constant axial tensile force T and a force distribution $F(x, t)$. The small-amplitude transverse motion of the string is described by the classic damped wave-equation:

$$m \frac{\partial^2 y_s}{\partial t^2} + \eta \frac{\partial y_s}{\partial t} - T \frac{\partial^2 y_s}{\partial x^2} = F(x, t) \quad (1)$$

where the wave speed is given by $c^2 = T/m$. Any solution of equation (1) can be formulated in terms of the string modal parameters: for modeshapes normalized at unitary maximum values modal masses are given as $m_n = m L/2, (\forall n)$. Other modal parameters are the circular frequencies $\omega_n = n\pi c/L$, damping values ζ_n and mode shapes $\varphi_n(x) = \sin(n\pi x/L)$, with $n = 1, 2, \dots, N$. The order N of modal truncation is problem-dependent and must be asserted by physical reasoning. On the modal space the forced response of the damped string is formulated as:

$$[M_s] \{\ddot{Q}_s(t)\} + [C_s] \{\dot{Q}_s(t)\} + [K_s] \{Q_s(t)\} = \{\Xi_s(t)\} \quad (2)$$

where $[M_s] = \text{Diag}(m_1, \dots, m_N)$, $[C_s] = \text{Diag}(2m_1\omega_1\zeta_1, \dots, 2m_N\omega_N\zeta_N)$ and $[K_s] = \text{Diag}(m_1\omega_1^2, \dots, m_N\omega_N^2)$ are the matrices of modal parameters, $\{Q_s(t)\} = \langle q_1(t), \dots, q_N(t) \rangle^T$ and $\{\Xi_s(t)\} = \langle \mathfrak{I}_1(t), \dots, \mathfrak{I}_N(t) \rangle^T$ are the vectors of modal responses and generalized forces, respectively. The damping values ζ_n are usually identified from experiments. The modal forces $\{\Xi_s(t)\}$ are obtained by projecting the external force field on the modal basis:

$$\mathfrak{I}_n(t) = \int_0^L F(x,t) \varphi_n(x) dx, (n = 1, 2, \dots, N) \quad (3)$$

The physical motion at any point of the string is computed from the modal amplitudes $q_n(t)$ by superposition:

$$y_s(x,t) = \sum_{n=1}^N \varphi_n(x) q_n(t) \quad (4)$$

and similarly concerning the velocities and accelerations. For given external excitation and initial conditions, the previous system of equations can be integrated using an adequate time-step integration algorithm.

Note that, although (2)-(4) obviously pertain to a linear formulation, nothing prevents us from including in $\mathfrak{I}_n(t)$ all nonlinear effects arising in the system. Accordingly, the system modes become coupled by the nonlinear effects. Explicit integration methods are well suited for the friction model used here. In this implementation, we used a simple Velocity-Verlet integration scheme.

For the present case, the external force field $F(x,t)$ is due to: (a) the excitation friction force $F_{s,a}(x_c,t)$ provided by the bow, which we will model in this paper as a single hair bow, although we can easily introduce excitation by a bow of finite width – see Inacio (2002); (b) the interaction force $F_b(x_b,t)$ between the body and the string at the bridge; (c) the interaction force $F_w(x_w,t)$ between the wolf eliminator and the string; (d) the interaction force $F_f(x_f,t)$ between the finger and the string at the fingerboard (see Figure 3).

The response of the body of the instrument can be represented by a simplified modal model:

$$[M_B] \{\ddot{Q}_B(t)\} + [C_B] \{\dot{Q}_B(t)\} + [K_B] \{Q_B(t)\} = \{\Xi_B(t)\} \quad (5)$$

where $[M_B]$, $[C_B]$ and $[K_B]$ are the matrices of the body modal parameters, $\{Q_B(t)\}$ and $\{\Xi_B(t)\}$ are the vectors of modal responses and generalized forces, respectively. The modal forces $\{\Xi_B(t)\}$ are obtained by projecting the string/body coupling force $F_b(x_b,t)$ on the body modal basis. The modal parameters are identified from a single transfer function measurement at the bridge. This fact leads to a requirement that the modal mass matrix should be normalized by postulating, for instance, that all modeshapes be unitary at the bridge location. The physical body motions at the bridge are then computed from the modal amplitudes by superposition.

The coupling between the string and the body of the violin arises from the bridge/string contact force $F_b(x_b,t)$ which is used in the previous equations. Following Inacio et al. (2008), we introduce a penalty model for this interaction by connecting the string to the bridge at location x_b through a very stiff spring (with a damper to minimize residual local oscillations). Then the force exerted by the body on the string is given as:

$$F_b(x_b,t) = K_{BS} [y_B(x_b,t) - y_s(x_b,t)] + C_{BS} [\dot{y}_B(x_b,t) - \dot{y}_s(x_b,t)] \quad (6)$$

where K_{BS} and C_{BS} are respectively the (high) stiffness and damping coupling coefficients between the body and the string at the bridge. $y_s(x_b,t)$ and $\dot{y}_s(x_b,t)$ are the displacement and velocity of the string at the bridge, $y_B(x_b,t)$ and $\dot{y}_B(x_b,t)$ are the displacement and velocity of the body at the bridge. Obviously, the same force (6) with opposite sign is exerted by the string on the body.

Wolf eliminator dynamics

The preceding computational strategy is easily extended to deal with wolf eliminators of the type shown in Figure 2. These are simply modeled as a mass M_w , with dynamics:

$$M_w \ddot{y}_w = F_w(t) \quad (7)$$

which is coupled to the string motion at location x_w , using a penalty formulation of the same type as (6). Then, the force exerted by the string on the eliminator is:

$$F_w(x_w,t) = K_{ws} [y_s(x_w,t) - y_w(t)] + C_{ws} [\dot{y}_s(x_w,t) - \dot{y}_w(t)] \quad (8)$$

while an identical and opposite force is exerted on the string by the device.

The coupling coefficients K_{ws} and C_{ws} depend on the internal structure of the wolf eliminator. A common type of wolf eliminators is designed such that the mass is directly applied to the string. Then K_{ws} will be high and C_{ws} low (typically of the same order of K_{BS} and C_{BS}). However, some wolf eliminators are coupled to the string through a

rubber nucleus. Then K_{ws} will be much lower and C_{ws} much higher than in the preceding case.

Finger control of the playing frequency

Introducing a “finger” to control the playing frequency is even simpler than previously described. At the finger location x_f , a nearly zero displacement is imposed, again using a penalty approach. The finite width of the finger is modeled by applying that such constraint at a number of points along the string – in the present case we used 3 points, at locations $x_{f_1} = x_f - W_f/2$, $x_{f_2} = x_f$ and $x_{f_3} = x_f + W_f/2$, where W_f is the assumed finger width. The coupling forces exerted on the string by the “discretized” finger are given as:

$$F_{f_j}(x_{f_j}, t) = -K_{fs} y_s(x_{f_j}, t) - C_{fs} \dot{y}_s(x_{f_j}, t) \quad ; \quad j = 1, 2, 3 \quad (9)$$

where K_{fs} and C_{fs} are empirical stiffness and damping coupling constants.

Bow excitation

The friction force arising between the string and the bow hair at the contact location x_c of the string is given by:

$$\begin{cases} F_s(x_c, t) = -\mu_d(\dot{y}_c) \frac{F_N}{b} \text{sgn}(\dot{y}_c) ; & \text{if } |\dot{y}_c| > 0 \\ |F_s(x_c, t)| < \mu_s \frac{F_N}{b} ; & \text{if } |\dot{y}_c| = 0 \end{cases} \quad (10)$$

where F_N is the normal force between the bow and the string, μ_s is a “static” friction coefficient (used during surface adherence), $\mu_d(\dot{y}_c)$ is a “dynamic” friction coefficient (used for sliding regimes) and b is the number of bow hairs used in the model. Here, the relative transverse velocity between the bow and the string is given by:

$$\dot{y}_c(t) = \dot{y}_s(x_c, t) - \dot{y}_{bow}(t) = \left[\sum_{n=1}^N \varphi_n(x_c) \dot{q}_n(t) \right] - \dot{y}_{bow}(t) \quad (11)$$

In this work we assume that $\mu_d(\dot{y}_c)$ is a function of the relative bow/string velocity, and use the following model:

$$\mu_d(\dot{y}_c) = \mu_d + (\mu_s - \mu_d) \exp(-C |\dot{y}_c|) \quad (12)$$

where μ_d is an asymptotic lower limit of the friction coefficient when $|\dot{y}_c| \rightarrow \infty$, and parameter C controls the decay rate of the friction coefficient with the relative bow/string sliding velocity. the friction model (12) can be readily fitted to typical experimental data, by adjusting the empirical constants μ_s , μ_d and C .

Computation of frictional forces is a delicate matter, often leading to numerical difficulties, in particular when dealing with stick-slip dynamical regimes. Details on the numerical implementation of the above friction formulation are provided in the paper by Inacio et al. (2008).

EXPERIMENTAL SET-UP AND PROCEDURE

Experimental set-up

This study was conducted on a German cello of the 19th century, which displays a “strong” wolf note when the G3 note is played, at approximately 196 Hz. The wolf note occurs on both the C and G strings and seems more prominent on the C-string.

During testing, the cello was in the vertical position, clamped by the neck to a rigid support with the endpin fixed on a rubber stopper. An accelerometer B&K 4375 was glued to the bridge close to the C-string corner, as shown in Figure 4. Also, a laser vibrometer Politec PVD 100 was used to measure the “dead” string-side motion, pointed between the bridge and the tailpiece – the laser dot can also be seen in Figure 4. A sound level meter and a camera were also used, respectively to measure the radiated sound pressure and to analyze the hand-bowing technique.

Five wolf-suppressors of two varieties were tested. They consist of a set of four solid brass masses of 5.3 g, 8.9 g, 10.9 g and 12.9 g, as well as a traditional brass cap with tightening screw and rubber core, the total mass being 14.9 g (see Figures 2 and 5). Each device was mounted at various locations on the “dead” side of the string, respectively at 1.5 cm, 4.0 cm, 7.5 cm and 11.0 cm below the bridge. The measured signals were digitized using a Siglab 4-channel acquisition system and then analyzed.



Figure 4. Set-up for the measurement of the bridge transverse dynamical responses and of the “dead” string-side motion.



Figure 5. Typical wolf-suppressor devices. Left: set of solid brass masses. Right: mass with rubber core and tightening screw.

Cello modal identification

In order to obtain the modal parameters of the cello body, which are used in our numerical simulations, a detailed

modal identification of the instrument body was performed from a transfer function measured at the bridge. As illustrated in Figure 6, the bridge was impacted from the A-string corner side, using a force transducer (B&K 8200) attached to a pendulum, to ensure repeatability in the measurements. The bridge response was measured at the C-string corner side, using the laser vibrometer and accelerometer. Measurements were performed keeping the strings of the instrument tensioned and in-tune but damped with a light cloth.



Figure 6. Experimental modal identification of the cello body through impact tests.

Extraction of the modal frequencies and damping values was performed from the bridge impulse response, using our implementation of the Eigensystem Realization Algorithm (ERA), which is a powerful identification algorithm in the time domain, see Juang & Pappa (1985) or Juang (1994). The cello modeshapes are assumed real and the body modal masses were obtained from the measured transfer function, as discussed earlier, by postulating that the corresponding modeshapes are unitary at the bridge location.

Test procedure for extracting wolf notes

The cello was hand-bowed by one of the paper co-authors, a violin maker who also has a strong experience as a musician. The study was conducted on both the C and G strings, which are cored strings with linear density of $14 \cdot 10^{-3}$ kg/m and $6.6 \cdot 10^{-3}$ kg/m, respectively.

For each wolf suppressor mounted on a given string and at each specific location, the experiment consisted in bowing the string to detect if any wolf note arises. To do so, the player was allowed to change the control parameters - bow velocity, bow normal force, bowing contact point and finger position. However, at the present time, no instrumentation was used to precisely monitor any of the bowing parameters. Therefore, no control of these parameters was exercised during the tests. When finding a wolf note, the musician attempted to maintain the applied normal force and bow velocity constant, as much as possible. A guess of the bow velocity can then be achieved by analyzing the test movies, from a set of markers drawn on the bow.

The bridge acceleration and the “dead” string velocity were digitized with a sampling frequency of 20 kHz, for recorded signals 4 sec long. From the bridge displacement signal, the playing and beating frequencies were identified. The measurement illustrated in Figure 1 is a typical amplitude modulated waveform of the bridge velocity, characteristic of a wolf note, measured when bowing the G string. After each test, it was also asked to the player to report a subjective

impression on the difficulty to extract a wolf note from the instrument, by using the terms “easy”, “difficult” or “no wolf”.

EXPERIMENTAL RESULTS

Modal identification results

A thorough modal identification of the cello body was performed on the impulse response $h_b(t)$ obtained from the bridge velocity signal. It was carried out in the 20 ~ 1500 Hz frequency range of the corresponding transfer function $H_b(\omega)$. Results show the existence of one main resonance at approximately 196 Hz, with relatively low damping. It is expected that this body mode will probably be responsible for the wolf note.

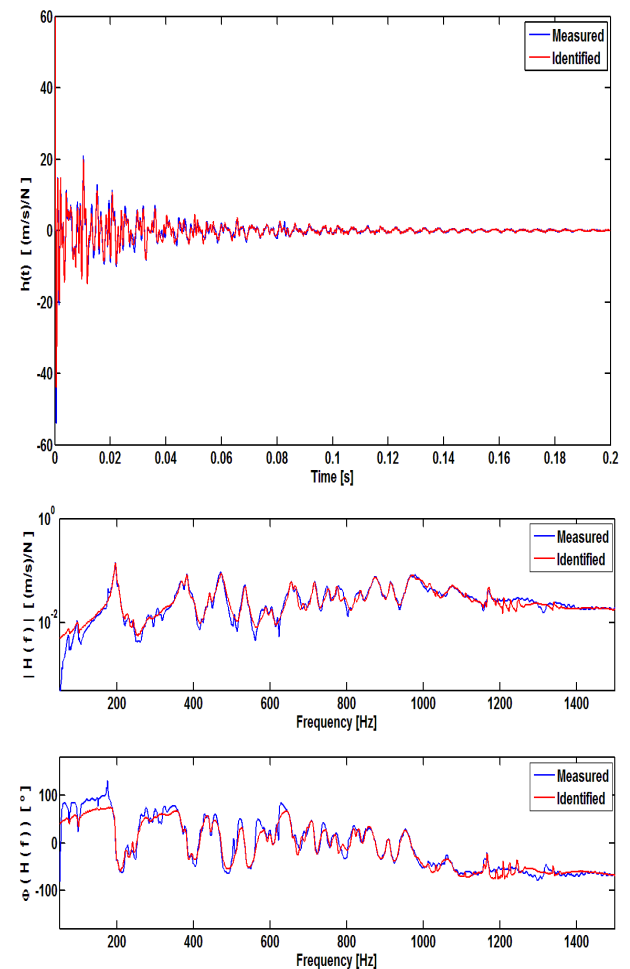


Figure 7. Measured (blue) and synthesized (red) impulse response (upper plot) and the corresponding transfer function amplitude (middle plot) and phase (lower plot), for the cello body.

The measured and synthesized (from 71 identified modes) impulse response and transfer function of the cello body are shown in Figure 7. Table 1 presents the modal parameters of the body, for several modes in the vicinity of the prominent resonance.

Table 1. Body modal frequencies and damping values in the vicinity of the most prominent body resonance.

Frequency (Hz)	152.1	167.3	195.9	202.0	225.7
Damping (%)	0.4	6.9	1.3	1.6	2.6

Stability charts of the wolf notes

Figures 8 and 9 present the wolf-occurrence maps obtained from the hand-bow experiments for the set of solid brass masses, mounted at the various locations on the C and G-strings respectively. The black dots locate the specific tested configurations (e.g., the wolf eliminator masses used and their attachment locations). A color scheme is used for highlighting the occurrence nature of the wolf note. The red and yellow colors stand for the cases for which it is respectively “easy” and “difficult” to establish a wolf note. The green color is used when “no wolf” has been obtained whatsoever, after many attempts. Also, the values of the wolf note frequencies and of the corresponding beating frequencies are displayed on the plots.

Results obtained for the C string shows that none of the tested solid mass eliminators suppressed the wolf tones, as depicted in Figure 8. The same conclusion applies when testing the wolf-suppressor with rubber core for all the tested locations. Thus, for the C string – which displays the most severe wolf note on the tested cello – no convenient solution was found to inhibit the wolf phenomenon. This feature confirms the erratic effectiveness of the devices and the laborious trial-and-error procedure to completely prevent the wolf phenomenon. At least, use of the devices sometimes render more difficult to maintain a wolf note. Actually, it appears that the closer to the bridge the wolf-suppressor location, the harder is the emergence of a wolf note. These test results are in agreement with the violin maker experience.

Somewhat surprisingly, Figure 8 also reveals that the wolf note frequency can change, as a result of the wolf suppressor additional mass, as well as of its location. For instance, there is an evident shift in the wolf-note frequency for solid masses mounted close to the bridge as seen in Figure 8. A plausible explanation could be that, due to the presence of the mass and the complexity of the body modal responses, the string vibration couples to other mode of the body cello. From Table 1, it seems plausible that the mode at 202 Hz, which has also small damping compared to other modes, would be responsible for the wolf note measured around 207 Hz. It should also be noted that for such situations, the wolf note is produced over a limited range on the fingerboard (less than one semitone) and that the musician denotes difficulties in obtaining the wolf note. Also, when the emergence of the wolf note is reported as “easy”, the unstable frequency is found close to the original wolf note frequency and usually occurs over consecutive positions on the fingerboard covering more than one tone. Looking at the beating frequencies, it seems that the more difficult is the emergence of the wolf note, the lower the beating frequency.

Figure 9 shows the stability map obtained for hand-bow experiments pertaining to the G string. Interestingly, two configurations prevent the wolf note efficiently. It occurs for the 5.3 g mass, when located near the bridge, in the first two positions (1.5 cm and 4.0 cm). The mass with rubber core also appears to be a good solution to suppress the wolf phenomenon when mounted close to the bridge. It should be noted that for the other locations, while a wolf note still occurs with the rubber mass, it is quite difficult for the musician to maintain the wolf note when the eliminator is located on the first three positions below the bridge.

Figure 9 also shows that locating the wolf suppressor close to the bridge has a strong influence on the value of the wolf frequency, as noted before for the C string. Actually, when

the solid masses 8.9 g, 10.9 g and 12.9 g are located close to the bridge, the wolf note frequency is significantly lower (between 155 Hz and 168 Hz). From Table 1, it seems possible that, in such cases, the string vibration is influenced by the body mode identified at 152.1 Hz. Also note that, for these configurations, the emergence of the wolf note is reported as “easy”.

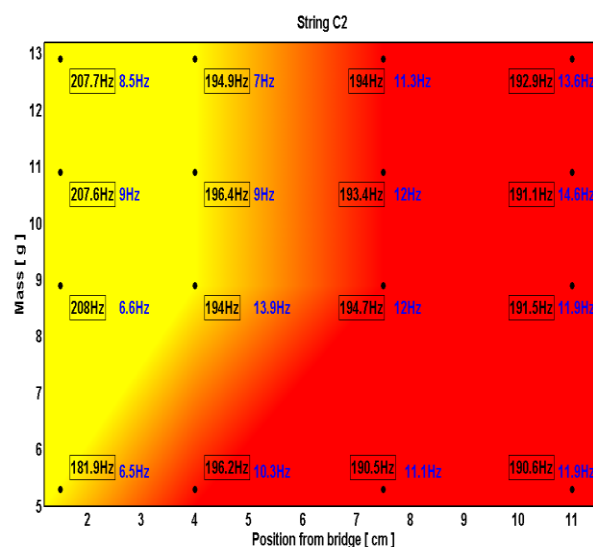


Figure 8. Wolf-occurrence map for the C string. The wolf note frequencies (black) and beating frequencies (blue) are shown as a function of the mass and location of the wolf suppressor.

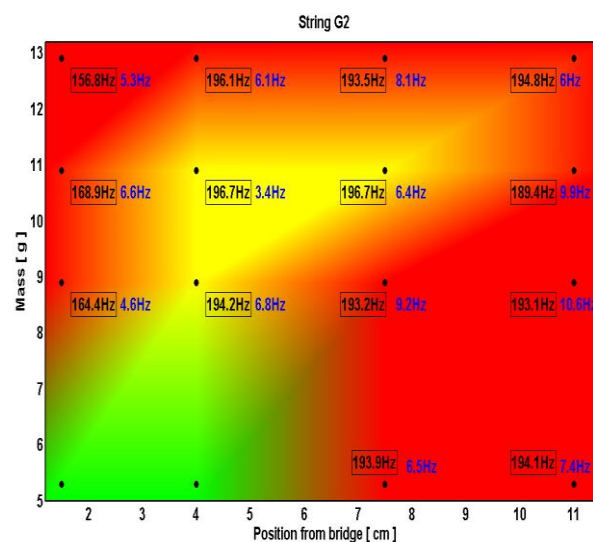


Figure 9. Wolf-occurrence map for the G string. The wolf note frequencies (black) and beating frequencies (blue) are shown as a function of the mass and location of the wolf suppressor.

ILLUSTRATIVE COMPUTATIONS

Bowing simulations were performed for both the C and G strings, with fundamental frequencies of 65.4 Hz and 97.9 Hz, respectively. The simulated cello strings have a total length of 0.83 m from the nut to the tailpiece, with an “active” length of 0.70 m from the bridge to the nut (the “dead” side is therefore 0.13 m). For simplicity, the strings were assumed perfect, so that natural frequencies are

harmonic. An average modal damping value of 0.1 % was used for all modes. In order to achieve adequate computational convergence, 80 string modes were used. The body of the cello was simulated using a modal basis of 45 modes, covering a frequency range up to 1000 Hz. Because of the explicit nature of the integration algorithm used, a small time-step $\Delta t = 10^{-6}$ sec was adopted.

All computations reported here were performed using the friction model (10), with the sliding law (12). Friction parameters are $\mu_s = 0.4$, $\mu_d = 0.2$ and $C = 5$. Furthermore, the following playing conditions are used: Normal bow force $F_N = 1$ N, tangential bow velocity $\dot{y}_{bow} = 0.1$ m/s and bowing location $x_c = 0.040$ m from the bridge. Finally, as in the real-life experiments, it proved quite useful to perform computations by simulating a slow ($T_{Slide} = 10$ sec) finger-glissando of a few centimetres along the string, in order to cover the possible wolf frequencies. Most of the computations covered the playing range 175 ~ 215 Hz. Beyond the typical signal processing of the computational results, we also performed estimates of the time-varying playing frequencies, which were identified using a zero-cross counting technique, within a moving window 0.1 sec wide.

Figure 10 shows the results obtained for an upward glissando on the C string, when no additional suppressor is used. In the complete time-domain response of the bridge, a wolf note clearly emerges between the finger positions $x_f \approx 0.379 \sim 0.367$ m, with a vibration frequency in the range 186 ~ 196 Hz. This result gives some confidence in the computational approach developed. In the lower plots, the details of the time-domain bridge responses show the usual Helmholtz regime (left plot), then a section of the wolf tone (center plot), as well as a low amplitude post-wolf regime (right plot). These show the complex dynamics of the bowed string, when strongly coupled to the body dynamics.

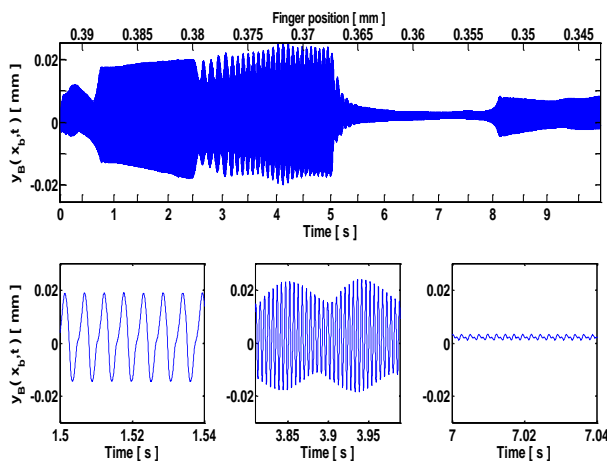


Figure 10. Time-domain bridge response for the bowed C string, with no wolf suppressor. Upper plot: complete glissando computation; Lower plots: details of the time-domain responses.

The results obtained when a mass of 8.9 g is applied respectively at 7.5 cm and 1.5 cm from the bridge are shown in Figures 11 and 12. Beyond the time-domain bridge responses, these results are also illustrated with plots of the

time-varying bridge frequencies. In Figure 11 one can notice the short initial transient, after which a typical Helmholtz regime arises, quickly leading to a wolf tone of increasing beating frequency. Notice that, in this case, use of the anti-wolf device actually *worsened* the problem, by extending the frequency range of the wolf-note.

At this stage, the dominant frequency is controlled by the first modal frequency of the string, which increases as the finger slides towards the bridge, in the range 182 ~ 196 Hz. It thus appears that, in the string/body coupled system, the string acts as the master subsystem and the body as the slave subsystem. As the finger keeps moving, the wolf note finally collapses and a higher-order regime of low amplitude settles for a while, which is dominated by the second and fourth modal frequencies. Then, the response amplitude increases again, with the response frequency controlled by the first and second modal frequencies of the string.

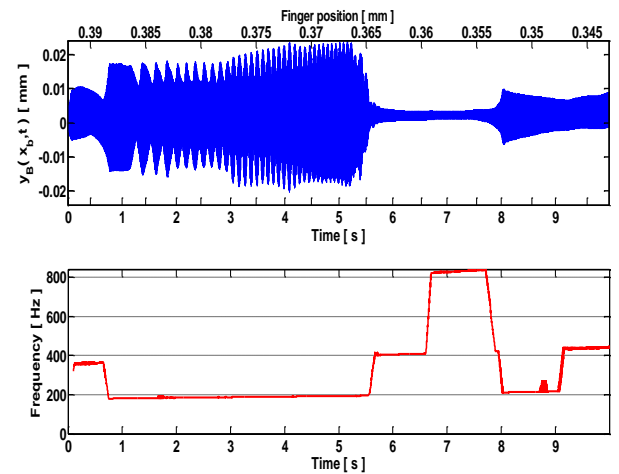


Figure 11. Time-domain bridge response for the bowed C string, with a mass 8.9 g located at 7.5 cm from the bridge (5.5 cm from the tailpiece). Upper plot: complete glissando computation; Lower plot: time-varying dominant frequency.

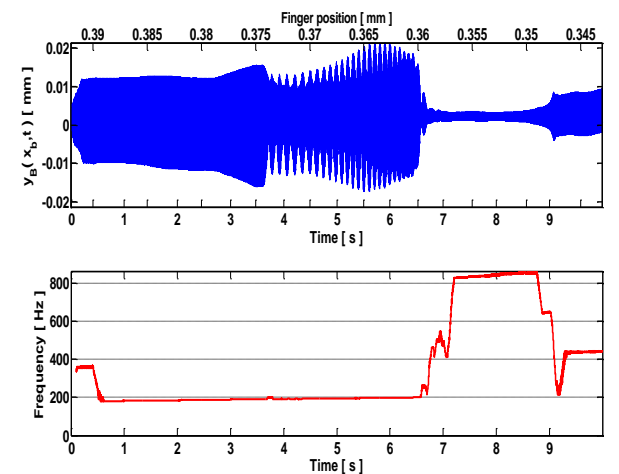


Figure 12. Time-domain bridge response for the bowed C string, with a mass 8.9 g located at 1.5 cm from the bridge (11.5 cm from the tailpiece). Upper plot: complete glissando computation; Lower plot: time-varying dominant frequency.

The results in Figure 12, when the wolf-eliminator mass is moved close to the bridge, follow a similar general pattern. However the range of frequency leading to a wolf note is narrower than in the preceding example. On the other hand,

the frequency of the wolf note is higher, in the range 190 ~ 200 Hz. It should be stressed that both features are qualitatively, and to some point even quantitatively, supported by the experimental results of Figure 8. Furthermore, these results also correlate well with the level of difficulty experienced by the musician to produce a wolf note in the corresponding experiments.

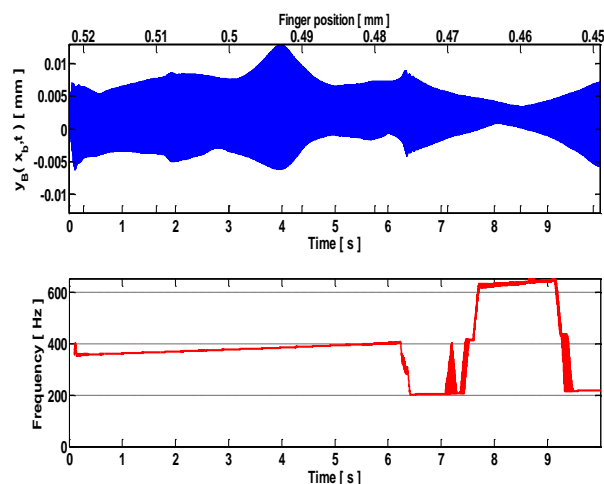


Figure 13. Time-domain bridge response for the bowed G string, with a mass 5.3 g located at 1.5 cm from the bridge (11.5 cm from the tailpiece). Upper plot: complete glissando computation; Lower plot: time-varying dominant frequency.

As a final illustration, Figure 13 shows the result obtained when the G string is simulated, when an anti-wolf device of 5.3 g is attached at 1.5 cm from the bridge. It can be seen that, for such computation, no wolf tone is ever generated – and this also is in agreement with the experimental results of Figure 9. Nevertheless, things are more complex than they appear, for in this case the numerical results display a response regime which is at “double-frequency” most of the time, in contrast to the basic Helmholtz regime which is most typically obtained.

CONCLUSION

In this paper we presented a series of hand-bow experiments performed on a cello, in order to characterize the occurrence of wolf note responses, their frequencies, as well as their relationship to the instrument body modes. These features were addressed in a systematic manner, in relation with the masses and attachment locations of a popular – but ill understood – “wolf-eliminator” device.

On the other hand, these experimental results were confronted with computations performed using a recently developed model for the highly nonlinear vibrations of bowed cello strings coupled to the instrument body, which incorporates as well the dynamics of the wolf-eliminator device. These computations display a generally satisfactory correlation with the experimental results. Furthermore, they enable a detailed analysis of the fully coupled system, which ultimately will lead to a better understanding of the wolf suppressing devices and their erratic effectiveness.

ACKNOWLEDGEMENTS

This Project is funded by the Portuguese Foundation for Science and Technology (FCT), through grant Ref. PTDC/FIS/103306/2008.

REFERENCES

- E. Gough (1980), “The resonant response of a violin G-string and the excitation of the wolf note”, *Acustica*, Vol. 44, pp. 113-123.
- O. Inacio, (2002) “Largeur d’Archet et Régimes Dynamiques de la Corde Frottée”, *Actes du 6ème Congrès Français d’Acoustique (6ème CFA)*, Lille, France.
- O. Inacio, J. Antunes (2008), “Wolf killing: The subtle problem of controlling cello string/body coupled resonances”. *Proceedings of the XXII ICTAM*, Adelaide, Australia, 25-29 August 2008.
- O. Inacio, J. Antunes, M. Wright (2008), “Computational modelling of string-body interaction for the violin family and simulation of wolf notes”. *Journal of Sound and Vibration* **310**, pp. 260-286.
- J. Juang (1994), “Applied System Identification”, *Prentice-Hall*, Englewood Cliffs, USA.
- J. Juang, R. Pappa (1985), “An eigensystem realization algorithm for modal parameter identification and model reduction”, *Journal of Guidance, Control and Dynamics* **8**, pp. 620-627.
- M. McIntyre, J. Woodhouse (1979), “On the fundamentals of bowed-string dynamics”, *Acustica*, Vol. 43, pp. 93-108.
- M. McIntyre, R. Schumacher, J. Woodhouse (1983), “On the oscillations of musical instruments”, *Journal of the Acoustical Society of America* **74**, pp. 1325-1345.
- J. Paud, R. Caussé, V. Gibiat (1991), “Quasi-périodicité et bifurcations dans la note de loup”, *J. Acoustique* **4**, pp. 253-259.
- J. Smith, J. Woodhouse (2000), “The tribology of rosin”, *Journal of the Mechanics and Physics of Solids* **48**, pp. 1633-1681.